

Elucidating the Inhibiting Mode of AHPBA Derivatives against HIV-1 Protease and Building Predictive 3D-QSAR Models

Xiaoqin Huang,^{†,‡} Liaosa Xu,[§] Xiaomin Luo,[†] Kangnian Fan,[§] Ruyun Ji,[†] Gang Pei,^{*,‡} Kaixian Chen,[†] and Hualiang Jiang^{*,†}

Center for Drug Design and Discovery, State Key Laboratory of Drug Research, Shanghai Institute of Materia Medica, Shanghai Institutes for Biological Sciences, Chinese Academy of Sciences, 294 Taiyuan Road, Shanghai 200031, People's Republic of China, Shanghai Institute of Biochemistry and Cell Biology, Shanghai Institutes for Biological Sciences, Chinese Academy of Sciences, 320 Yueyang Road, Shanghai 200032, People's Republic of China, and Department of Chemistry, Fudan University, Shanghai 2000437, People's Republic of China

Received June 18, 2001

The Lamarckian genetic algorithm of AutoDock 3.0 has been used to dock 27 3(*S*)-amino-2(*S*)-hydroxyl-4-phenylbutanoic acids (AHPBAs) into the active site of HIV-1 protease (HIVPR). The binding mode was demonstrated in the aspects of the inhibitor's conformation, subsite interaction, and hydrogen bonding. The data of geometrical parameters (τ_1 , τ_2 , and τ_3 listed in Table 2) and root mean square deviation values as compared with the known inhibitor, kni272,²⁸ show that both kinds of inhibitors interact with HIVPR in a very similar way. The r^2 value of 0.860 indicates that the calculated binding free energies correlate well with the inhibitory activities. The structural and energetic differences in inhibitory potencies of AHPBAs were reasonably explored. Using the binding conformations of AHPBAs, consistent and highly predictive 3D-QSAR models were developed by performing CoMFA, CoMSIA, and HQSAR analyses. The reasonable r_{cross}^2 values were 0.613, 0.530, and 0.717 for CoMFA, CoMSIA, and HQSAR models, respectively. The predictive ability of these models was validated by kni272 and a set of nine compounds that were not included in the training set. Mapping these models back to the topology of the active site of HIVPR leads to a better understanding of vital AHPBA–HIVPR interactions. Structural-based investigations and the final 3D-QSAR results provide clear guidelines and accurate activity predictions for novel HIVPR inhibitors.

Introduction

Acquired immunodeficiency syndrome (AIDS) is the first major epidemic caused by human immunodeficiency virus type (HIV), a member of the retroviruses family.¹ Analysis of the nucleotide sequence of HIV-1 genome leads to the discovery that the virus encodes an aspartic protease.^{2,3} Interaction of the HIV-1 protease (HIVPR) by either mutation or chemical inhibition results in the production of immature, noninfectious viral particles; thus, the function of this enzyme is shown to be essential for proper virion assembly and maturation.^{4–6} It is not surprising that HIVPR is identified as the prime target for structure-based drug design,^{7,8} and the importance of HIVPR inhibitors in the treatment of AIDS has been well-established.⁹ More recent advances in inhibitor design have focused on structural modification to improve their inhibitory potency and oral bioavailability and to circumvent drug resistances.^{10–13} Despite these successes, it is nearly impossible to treat all of the growing worldwide AIDS population based on currently available drugs, so the need for inexpensive and widely available HIVPR inhibitors still exists.

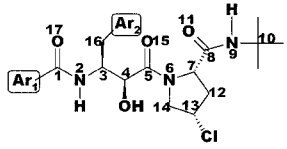
AHPBA (3(*S*)-amino-2(*S*)-hydroxyl-4-phenylbutanoic acid) and its derivatives (AHPBAs), which are the transition state mimics of HIVPR substrates,¹⁴ are totally new lead compounds as inhibitors to HIVPR and have been shown potent inhibitory activity against HIVPR.^{15–17} Some of them also have high anti-HIV activities; compound **20** (Table 1) is the most potent (IC₅₀ is 0.8 nM and IC₉₀ CEM/HIV-1 IIIB is 27nM) and has demonstrated good pharmacokinetics in rats.¹⁷ Structure–activity relationships of AHPBAs show that these compounds possess strong potency and good enzyme selectivity.¹⁶ The lipophilic aromatic ring system, which fits into the S₁ hydrophobic pocket of HIVPR, is demonstrated to be very important.¹⁸ The X-ray structure determination together with the molecular dynamic simulations^{13,19} revealed the atomic details of inhibitor-induced conformational changes and also the essential role of structural subunits for the catalytic activity of HIVPR. These structure-based approaches are approved to be valuable for dynamic optimization of inhibitors against HIVPR but could not lead to predictive models for structural modification or new inhibitor designing. Some meaningful clues from QSAR studies on cyclic cyanoguanidines²⁰ were obtained for the selection of positional substituents according to their physical chemistry properties. Without the investigation about conformation space of inhibitors and their binding mechanism with HIVPR, it remains speculative whether these semiempirical models could be used as practical tools for designing better analogues with superior

* To whom correspondence should be addressed. Tel: +86-21-64311833 ext. 222. Fax: +86-21-64370269. E-mail: H.J., hljiang@mail.shcnc.ac.cn, jiang@iris3.simm.ac.cn; G.P., gpei@sibs.ac.cn.

[†] Shanghai Institute of Materia Medica, Shanghai Institutes for Biological Sciences, Chinese Academy of Sciences.

[‡] Shanghai Institute of Biochemistry and Cell Biology, Shanghai Institutes for Biological Sciences, Chinese Academy of Sciences.

[§] Fudan University.

Table 1. Compounds and Their HIVPR Inhibitory Activity


No.	Ar ₁	Ar ₂	IC ₅₀ (nM)	-log IC ₅₀	No.	Ar ₁	Ar ₂	IC ₅₀ (nM)	-log IC ₅₀
1			8.2	8.10	18			1.2	8.92
2			1.3	8.89	19			3.2	8.49
3			1.7	8.77	20			0.8	9.10
4			2.5	8.60	21			2.8	8.55
5			3.5	8.46	22			1.2	8.92
6			1.9	8.72	23			0.8	9.10
7			2.1	8.68	24			26	7.59
8			4.6	8.34	25			11	7.96
9			6.3	8.20	26			12	7.92
10			3.9	8.41	27			3.6	8.44
11			2.5	8.60	1*			1000	6.00
12			1.3	8.89	2*			1000	6.00
13			33	7.50	3*			39	7.41
14			8.6	8.10	4*			9.0	8.05
15			3.6	8.44	5*			1.5	8.82
16			49.9	7.30	6*			3.4	8.47
17			34.3	7.46	7*			1.3	8.89
					8*			5.4	8.27
					9*			14	7.85

* Compounds that were not included in the construction of 3D-QSAR models.

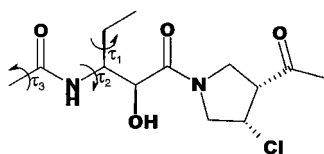
pharmacokinetic and efficacy profiles. Developing 3D-QSAR models under the guide of information from the catalytic site of enzymes²¹ has been proven as one of the more rational methodologies for binding affinity prediction of new inhibitors.

Taking account of the pioneering works in the field of designing and synthesis of HIVPR inhibitors, it becomes fascinating for us to study the inhibitory mechanism of AHPBAs against HIVPR and investigate the three-dimensional quantitative structure–activity relationships (3D-QSAR) of AHPBAs. To the best of our knowledge, there has been no previous effort carried out to seek new insight into the relationship between the structure information and the inhibitory potency of AHPBAs at the level of binding free energy prediction, especially by theoretical methods, such as automated molecular docking, comparative molecular field analysis (CoMFA),²² comparative molecular similarity analysis (CoMSIA),²³ and hologram quantitative structure–activity relationship (HQSA)²⁴ approaches.

The aim of the present research is to demonstrate the common binding mode of AHPBAs with HIVPR and to predict the binding free energies relative to the inhibitory potencies of these compounds. The further important goal is to obtain not only stable and predictive but also fast and convenient QSAR models, which are located at the 3D level about the main intermolecular interactions involved in the HIVPR inhibition.

Computational Details

To test the reliability of the Tripos force field encoded in the Sybyl 6.5 software package,²⁵ the geometry of the AHPBA structural template (Formula 1) was optimized by an ab initio Hartree–Fock self-consistent field method along with the standard polarized double- ζ bases set (6-31G**).²⁶ The Tripos force field optimized structure of AHPBAs fit well with the structure derived from the ab initio method. Thus, the initial structures of the 27 AHPBA compounds (Table 1) were built based on the skeleton of Formula 1 and then subjected to minimization using Tripos force field and Gasteiger–Hückel charges;²⁷ a nonbond cutoff of 8 Å was adopted to consider the intramolecular interaction. All of the calculations were performed on a Silicon Graphics Indigo XZR 10 000 workstation.



Formulae 1

1. Molecular Docking. The crystal structure of HIVPR in complex with its inhibitor (kni272) was recovered from Brookhaven Protein Database (entry code 1HPX).²⁸ Missing side chains of the HIVPR 3D structure were added using the fragment library of the Biopolymer module in Sybyl 6.5.²⁵ The potential of the HIVPR 3D structure was assigned according to Amber 4.0 force field with Kollman-all-atom charges, and it was further checked by the Procheck function in Insight II²⁹ to correct some unfavorable φ and ψ values of the amino acids.

For the reason of tackling the interacting mode of AHPBAs with HIVPR, the advanced docking program AutoDock 3.0³⁰ was used to perform the automated molecular docking. The Lamarckian genetic algorithm (LGA)³⁰ was applied to deal with the AHPBA–HIVPR interactions. Briefly, the LGA described the relationship between AHPBA and HIVPR by the translation, orientation, and conformation of AHPBA. These so-called “state variables” were the AHPBA’s genotype, and the resulting atomic coordinates together with the interaction and the intramolecular energies were the AHPBA’s phenotype. The environmental adaptation of AHPBA’s phenotype was reverse-transcribed into its genotype and became heritable traits. Each docking cycle, or generation, consisted of a regimen of fitness evaluation, crossover, mutation, and selection. A Solis and Wets local search³¹ performed the energy minimization on a user-specified proportion of the population. The docked structures of AHPBAs were generated after a reasonable number of evaluations. The whole docking operation could be stated as follows.

First, the HIVPR molecule was checked for polar hydrogens and partial atomic charges, the PDBQs format file was created, and the atomic solvation parameters were also assigned for this macromolecule. In the meanwhile, all of the torsion angles of AHPBAs were defined in order to be explored during molecular docking. This allowed the conformational search of AHPBA during the process of docking.

Second, the 3D grid was created by the AutoGrid algorithm³⁰ to evaluate the interacting energy between the AHPBAs and the HIVPR. In this stage, the HIVPR was embedded in the 3D grid and a probe atom was placed at each grid point. The affinity and electrostatic potential grid were calculated for each type of atom in AHPBA molecules. The energetics of a particular AHPBA configuration was found by trilinear interpolation of affinity values and electrostatic interaction of the eight grid points surrounding each of the atoms in AHPBA.

Third, a series of the docking parameters were set on. Not only the atom types but also the generations and the number of runs for the LGA algorithm were edited and properly assigned according to the requirement of the Amber force field. The number of generation, energy evaluation, and docking runs was set to 370 000, 1 500 000, and 10, respectively. The kinds of atomic charges were taken as Kollman-all-atom³² for HIVPR and Gasteiger–Hückel²⁷ for AHPBAs.

Finally, the docked complexes of AHPBAs–HIVPR were selected according to the criteria of interacting energy combined with geometrical matching quality. These complexes were used as the starting conformation for further energetic minimization and geometrical optimization before the final models were achieved.

2. Binding Free Energy Prediction. Typically, three binding energy terms used in the previous versions of AutoDock³³ were included in the score function: the van der Waals interaction represented as a Lennard–Jones 12–6 dispersion/repulsion term, the hydrogen bonding represented as a directional 12–10 term, and the Coulombic electrostatic potential. So, the binding energy of AHPBAs with HIVPR could be simply

described as the electrostatic, van der Waals, and hydrogen bonding interaction energy, respectively.

On the basis of the traditional molecular force field model of interaction energy, a new score function at the level of binding free energy was derived and adopted in the version of AutoDock 3.0.³⁰ Not only the restriction of internal rotors, the global rotation, and translation were modeled depending on the number of torsion angles of the ligand but also the desolvation upon binding and the hydrophobic effect (solvent entropy changes at solute–solvent interfaces) were calculated. The total binding free energy was empirically calibrated based on the above-stated terms and a set of coefficient factors.³⁰ Thus, the new score function was sufficient to rank the inhibitors in the different levels of binding affinities.

The same rationale was applied to the system of AHPBAs–HIVPR in order to evaluate the binding properties more precisely than the traditional molecular mechanics method did, and the total binding free energy between AHPBAs and HIVPR was calculated according to the algorithm in the AutoDock 3.0 program.³⁰

3. 3D-QSAR Studies. To more fully explore the specific contributions of electrostatic, steric, and hydrophobic effects in the binding of AHPBAs to HIVPR and to build predictive QSAR models, CoMFA,²² CoMSIA,²³ and HQSAR²⁴ studies were performed by using the conformations and their alignment at the binding site of the HIVPR, which resulted from the molecular docking.

3.1. CoMFA. Usually, steric and electrostatic field energies were probed using an sp^3 carbon atom and a +1 net charge atom, respectively. Steric and electrostatic interactions were calculated using a Tripos force field with a distance-dependent dielectric constant at all intersections in a regularly spaced (2 Å) grid. The minimum- σ (column filtering) was set to 2.0 kcal/mol to improve the signal-to-noise ratio by omitting those lattice points whose energy variation was below this threshold. A cutoff of 30 kcal/mol was adopted, and the regression analysis was carried out using the partial least-squares (PLS) method. The final model was developed with the optimum number of components equal to that yielding the highest r_{cv}^2 .

3.2. CoMSIA. Three physicochemical properties, steric, electrostatic, and hydrophobic fields, have been evaluated. The steric contribution was reflected by the third power of the atomic radii of the atoms. Electrostatic properties were introduced as atomic charges that resulted from molecular docking. An atom-based hydrophobicity was assigned according to the parametrization developed by Viswanadhan et al.³⁴ The lattice dimensions were selected with a sufficiently large margin (>4 Å) to enclose all aligned molecules. Any singularities were avoided at atomic positions in CoMSIA fields because a Gaussian type distance dependence of the physicochemical properties was adopted; thus, no arbitrary cutoffs were required. In general, similarity indices ($A_{F,K}$) between the compounds of interest and a probe atom placed at the intersections of the lattice could be calculated with eq 1

$$A_{F,K}^q(j) = - \sum_{i=1}^n w_{\text{probe},k} w_{ik} e^{-ar_{iq}^2} \quad (1)$$

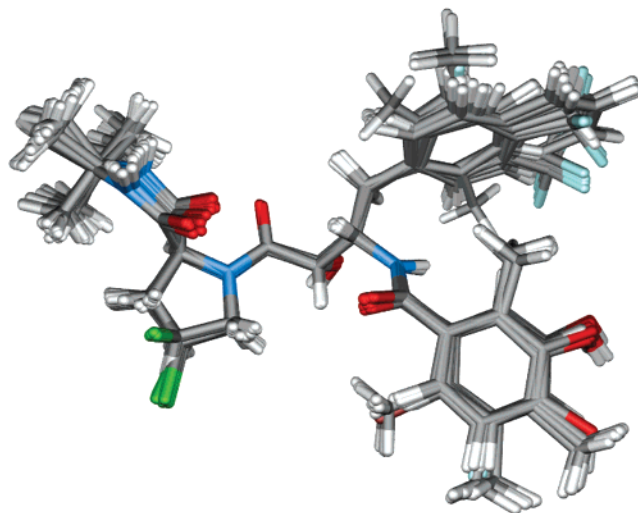


Figure 1. Probable binding conformations of AHPBAs and their alignment in the binding site of HIVPR.

where q represents a grid point; i is the summation index over all atoms of the molecule j under computation; w_{ik} is the actual value of the physicochemical property k of atom i ; and $w_{\text{probe},k}$ is the value of the probe atom. In the present study, similarity indices were computed using a probe atom ($w_{\text{probe},k}$) with a charge of +1, a radius of 1 Å, a hydrophobicity of +1, and an attenuation factor α 0.3 for the Gaussian type distance. The statistical evaluation for the CoMSIA analyses was performed in the same way as described in CoMFA.

3.3. HQSAR. The construction of a molecular hologram containing the HQSAR descriptors was completed as following this procedure: at first, the molecule was hashed to a molecular fingerprint that encoded the frequency of occurrence of various molecular fragment types using a predefined set of rules. Then, the molecular fingerprint was cut into strings at a fixed interval as specified by a hologram length (HL) parameter, and at last, all of the generated strings were hashed into a fixed length array. The Sybyl line notation for each string was mapped to a unique integer in the range of 0–2³¹ using a cyclic redundancy check algorithm. The numerical representation of molecules was exploited by a subsequent correlation analysis; typically, a PLS QSAR model was constructed. The optimal HQSAR model was constructed by screening the 12 default HL values, which were a set of prime numbers ranging from 53 to 401.

Results and Discussion

1. Interacting Mode with HIVPR. 1.1. Inhibitor's Conformation. Figure 1 illustrates the probable binding conformations for the 27 AHPBAs extracted from AHPBA–HIVPR complexes. Figure 2A shows the 3D model of the AHPBAs–HIVPR complex, and Figure 2B is the conformational comparison for the most potent inhibitors, compound **12** (Table 1) and compound kni272.²⁸ The main conformational difference between the AHPBAs and the kni272 could be represented as the three torsion angles (τ_1 , τ_2 , and τ_3 in Formula 1) and the root mean square deviation (RMSD) values based on the parts of similar structure including the Ar₂ group. These data are summarized in Table 2 and shown in Figure 2C. Figure 3 generally represents the interacting

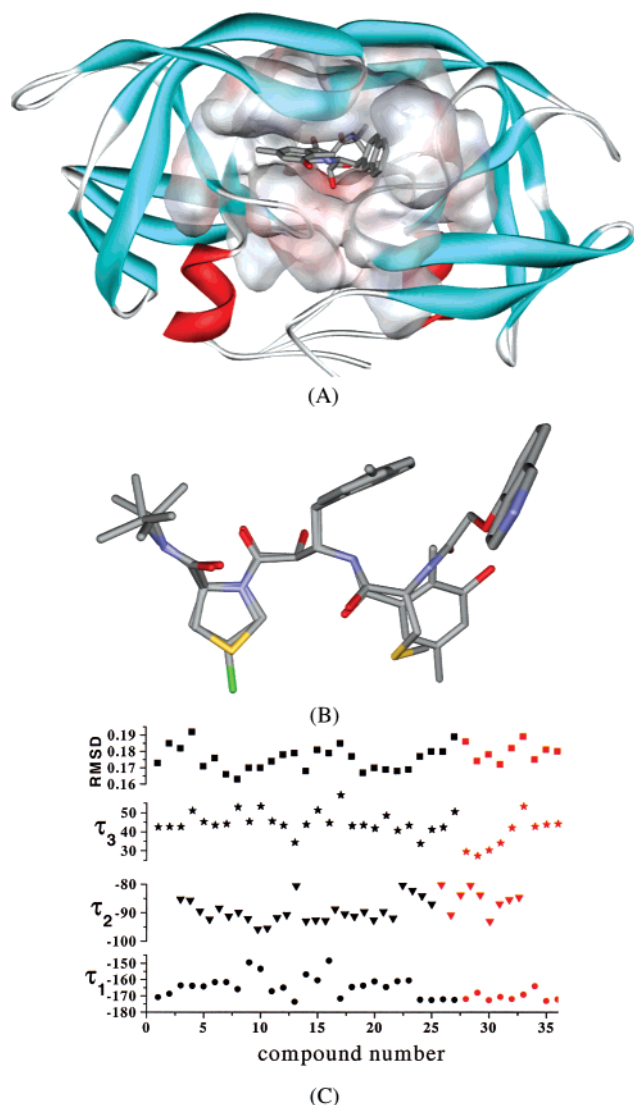


Figure 2. 3D-model of the AHPBA-HIVPR complex. (A) Cartoon representation of the AHPBA-HIVPR structural model. (B) The conformational comparison for one of the potential inhibitors, compound **12**, and kni272 in the crystal structure;²⁸ all of the molecules are shown in stick style, and the hydrogen atoms are hidden. (C) The geometrical parameters (τ_1 , τ_2 , and τ_3) and RMSD values of AHPBAs as compared with kni272; red-colored points are of the testing set. (A) and (B) are reproduced from the POV-Ray³⁹ program.

mode of AHPBAs with HIVPR. Just like the inhibitor kni272²⁸ and most of the other transition state mimic inhibitors cocrystallized with HIVPR,^{35,36} AHPBAs locate in the center of the typical binding pocket of HIVPR and share some common binding features for each other. All of the AHPBAs are bound in the active site of HIVPR in an extended conformation (Figures 1 and 2A), and the binding conformations of AHPBAs could be aligned quite well overall. Following a similar binding pattern with compound kni272,²⁸ the Ar₂ group (Table 1) of all of the 27 AHPBAs is situated at the S₁ subsite of the binding pocket, and the Ar₁-CONH group occupies the S₂ subsite. Meanwhile, the NH-tertiary butyl group interacts with the S₂' subsite, and the proline-CO part is in match with the S₁' subsite.

1.2. Subsite Interactions. The open mouth of the small hydrophobic pocket formed by residues Leu23', Gly48, Gly49, Ile50, Pro81', Val82', and Ile84' of HIVPR

Table 2. Geometrical Parameters of AHPBAs Binding Conformations and RMSD Values as Compared with kni272 from Crystal Structure 1HPX²⁸

compd	τ_1 (°)	τ_2 (°)	τ_3 (°)	RMSD
1	-170.9	-85.2	42.5	0.173
2	-168.8	-85.6	42.7	0.185
3	-163.7	-89.5	42.7	0.182
4	-163.9	-92.3	51.1	0.192
5	-164.3	-88.4	45.3	0.171
6	-161.7	-91.2	43.5	0.176
7	-161.7	-89.9	44.2	0.166
8	-166.0	-92.1	52.9	0.163
9	-149.6	-95.8	45.4	0.170
10	-153.4	-95.5	53.4	0.170
11	-167.3	-91.8	45.6	0.174
12	-165.0	-90.7	43.4	0.178
13	-173.7	-80.6	34.4	0.179
14	-156.9	-92.9	43.8	0.168
15	-160.5	-92.6	51.4	0.181
16	-148.5	-92.8	44.7	0.179
17	-171.8	-88.7	59.3	0.185
18	-164.6	-90.5	43.1	0.177
19	-163.8	-91.3	43.5	0.167
20	-161.3	-89.7	41.8	0.170
21	-164.7	-92.6	48.5	0.169
22	-161.1	-89.7	40.8	0.168
23	-160.7	-91.9	43.4	0.169
24	-172.4	-80.4	33.8	0.177
25	-172.7	-82.2	41.2	0.180
26	-172.2	-84.1	42.3	0.180
27	-172.5	-87.0	50.6	0.189
1*	-172.1	-80.3	29.4	0.186
2*	-168.2	-90.9	27.2	0.174
3*	-172.8	-83.9	30.2	0.178
4*	-170.8	-80.5	34.0	0.172
5*	-172.1	-83.9	42.0	0.182
6*	-169.4	-93.1	53.2	0.189
7*	-164.2	-87.0	42.7	0.175
8*	-173.3	-85.5	43.7	0.181
9*	-172.3	-84.7	44.1	0.180

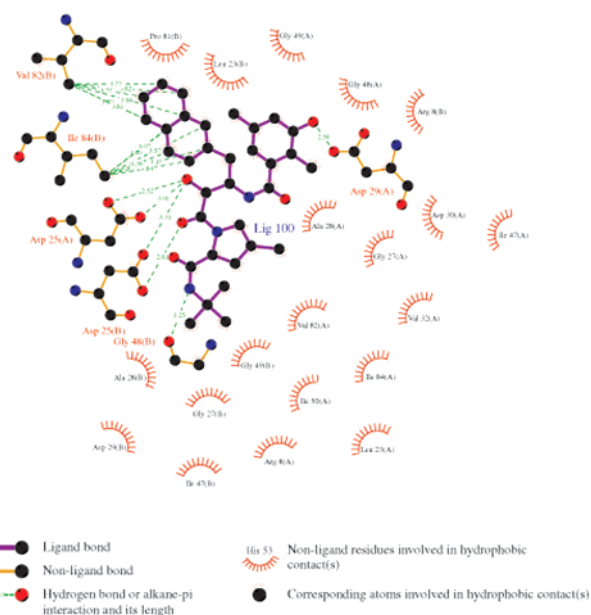


Figure 3. 2D representative for the general interacting mode of AHPBAs (compound **20** as a representative) with HIVPR; it is drawn by LIGPLOT.⁴⁰

is directly toward the Ar₂ group and wraps the most part of the latter (Figure 3). They interact with each other tightly through hydrophobic interaction. The outside edge of the Ar₂ group is almost blocked off by the hydrogen network formed between Arg8' and Asp29. Interestingly, the two terminal methyl groups of the side

chains of residues Val82' and Ile84', respectively, interact with the two aromatic rings of the Ar₂ group of compound **20** or the benzyl ring of the other inhibitors through nonpolar alkane- π interaction³⁷ (Figure 3). This kind of alkane- π interaction has not yet been appreciated in inhibitor-enzyme binding. To estimate the strength of the alkane- π interaction, we performed a theoretical calculation employing the ab initio quantum chemistry methods of Møller-Plesset second-order correlation method (MP2)³⁸ at the 6-31G* basis set level, taking methane-benzene as model systems. The distance between the methyl carbon and the center of benzene is 3.7 Å, which is in agreement with the distances of the two methyl carbons to the centers of the two rings of Ar₂ (Figure 3). The binding energy of MP2/6-31G* between methyl and benzene is -1.3 kcal/mol. This indicates that the alkane- π interaction contributes about 2.6 kcal/mol energy for compound **20**-HIVPR binding, or at least 1.3 kcal/mol energy for the other compounds-HIVPR binding, and points out the importance of the aromaticity of Ar₂.

The Ar₁-CONH group binds with the side chains of residues Ala28, Asp29, Asp30, Val32, Ile47, Gly48, and Ile84 of HIVPR through not only hydrophobic interaction but also electrostatic interaction to some extent. The carbonyl group (>C=O) of residue Gly48 is in a position almost perpendicular to the plane of the aromatic ring of the Ar₁ group. The distance from the carbonyl oxygen of Gly48 to the center of the aromatic ring of the Ar₁ group is 3.51 Å. So, the residue Gly48 may be one of the important factors determining the 3D positioning of the Ar₁ group in the binding pocket.

The NH-tertiary butyl group at the other end of the AHPBA molecules is surrounded by residues Gly27', Ala28', Asp29', Ile47', Gly48', Gly49', and Ile50 of HIVPR. Although the hydrophobic space is not fully occupied by the tertiary butyl group, they are in good geometrical match through the side chains of Ala28' and Ile50. The proline-CO group of AHPBAs situates in a small hydrophobic pocket of the subsite S₁' and interacts with the side chains of residues Leu23, Val82, and Ile84 of HIVPR; the chloride points directly to the gap between Leu23, Val82, and Ile84.

1.3. Hydrogen-Bonding Interactions. Another important characteristic of the interaction between AHPBAs and HIVPR is the hydrogen bonding (Figure 3). There are several hydrogen bonds formed between the AHPBAs and the side chains of some residues in HIVPR. The hydroxyl group at position 4 of AHPBAs (Table 1) could form hydrogen bonds with O ^{δ 1} and O ^{δ 2} atoms of Asp25 or O ^{δ 2} of Asp25', and the >C=O group at position 5 (Table 1) forms a hydrogen bond with the protonated O ^{δ 1} of Asp25'. This network of hydrogen bonds in the catalytic site of HIVPR must play a vital role in determining the level of binding affinities for AHPBAs with HIVPR, and this may be the important reason why the AHPBAs could inhibit the HIVPR much more potently. The oxygen atom of the hydroxyl group at Ar₁ might be an acceptor to form a hydrogen bond with the -NH group at the backbone of residue Asp29 on one hand; the hydrogen atom of the hydroxyl group at Ar₁ hydrogen bonds with O ^{δ 1} of the same residue on the other hand. These hydrogen bonds greatly strengthen the interaction of the aromatic ring Ar₁ with the

Table 3. Predicted Binding Free Energy (kcal/mol) vs the Experimental Activity (-logIC₅₀) of AHPBAs and kni272

compd	-logIC ₅₀	ΔG (kcal/mol)	compd	-logIC ₅₀	ΔG (kcal/mol)
1	8.10	-14.81	19	8.49	-15.02
2	8.89	-15.31	20	9.10	-16.02
3	8.77	-15.48	21	8.55	-14.96
4	8.60	-15.01	22	8.92	-15.26
5	8.46	-15.25	23	9.10	-15.05
6	8.72	-15.28	24	7.59	-14.05
7	8.68	-15.15	25	7.96	-14.15
8	8.34	-15.03	26	7.92	-13.91
9	8.20	-14.90	27	8.44	-14.92
10	8.41	-14.98	1*	6.00	-11.18
11	8.60	-15.18	2*	6.00	-11.29
12	8.89	-15.66	3*	7.41	-13.31
13	7.50	-13.60	4*	8.05	-14.42
14	8.10	-14.76	5*	8.82	-15.08
15	8.44	-14.93	6*	8.47	-15.06
16	7.30	-13.67	7*	8.89	-15.40
17	7.46	-13.86	8*	8.27	-14.78
18	8.92	-15.50	9*	7.85	-13.89

surrounding hydrophobic field produced by side chains of residues Ala28, Val32, Ile47, and Ile84 in HIVPR. Interestingly, the -NH group at position 9 of AHPBAs also forms a hydrogen bond with the >C=O group of residue Gly48' in HIVPR. This hydrogen bonding intensely determines the 3D space position of the tertiary butyl group in the binding pocket and stabilizes the hydrophobic interaction of the tertiary butyl group with the side chains of residues Ala28', Ile47', and Ile50 in HIVPR.

On further inspection of the AHPBA-HIVPR complex model, the >C=O groups at positions 1 and 8 of AHPBAs are located adjacent to the -NH groups of Ile50/Ile50'. The distances between them are within 4 Å, and the conformation of this part in the complex is symmetric to some extent. There may be a hydrogen bond network formed between the >C=O groups at positions 1 and 8 of AHPBAs and the -NH groups of Ile50/Ile50' through a water molecule if the complex is crystallized. This is just like the hydrogen bonding tetrahedral network and a water molecule named as Wat301 found in the kni272-HIVPR²⁸ and other inhibitor-HIVPR crystal structures.^{41,42}

As a whole, the AHPBAs interact with HIVPR through a hydrophobic, hydrogen bonding interaction and a local, weak electrostatic interaction. The hydroxyl group at position 4 of AHPBAs is located at the center of the electrostatic field produced by the negatively charged side chains of an active catalytic triad of HIVPR. The binding of the AHPBAs may introduce significant influence on the conformation of those regions that define the binding site of HIVPR, and the different ionization states of the catalytic aspartyl groups of Asp25 and Asp25'. The presence of the inhibitor makes the dimeric structure of HIVPR stabilized, especially the flap region that becomes conformationally closed.^{43,44}

2. Correlation between Binding Free Energy and Inhibitory Activity. Table 3 lists the predicted binding free energy of AHPBAs with HIVPR. Satisfied that the 3D structures of the AHPBA-HIVPR complexes were practically reasonable, the multiple regression analysis⁴⁵ was performed to explore whether the inhibitory potencies of AHPBAs could be correlated with the energetic information. The regression equation was

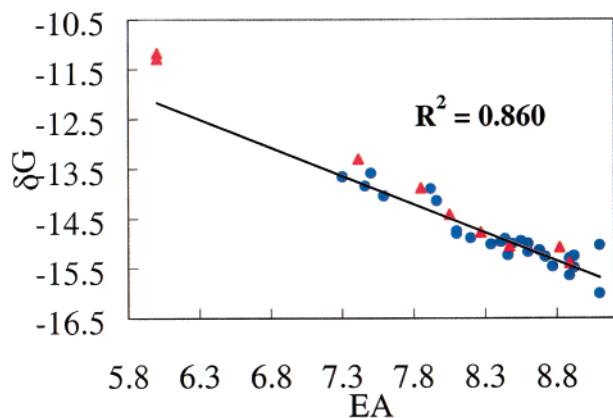


Figure 4. Correlation between the binding free energy (ΔG , kcal/mol, $T = 298.15$ K) of AHPBAs (\bullet , compounds of the training set; \blacktriangle , compounds of the testing set) with the HIVPR and the experimental inhibitory potencies ($-\log IC_{50}$).

Table 4. Statistical Indexes of CoMFA, CoMSIA, and HQSAR Models Based on AHPBA Binding Conformers

	cross-validated		conventional		
	r_{cross}^2	optimal comp	r^2	s	$F_{6,20}$
CoMFA	0.613	5	0.978	0.085	149.159
CoMSIA	0.530	6	0.970	0.100	106.709
steric (S)	0.349	6	0.951	0.127	65.344
electrostatic (E)	0.366	3	0.825	0.241	15.682
hydrophobic (H)	0.422	6	0.949	0.130	61.861
HB acceptor	0.453	5	0.818	0.246	14.966
HB donor	0.373	2	0.782	0.269	11.960
HQSAR	0.717	5	0.950	0.128	307 (BL) ^a

^a Best length in the HQSAR model.

obtained for the inhibitory potencies, $-\log IC_{50}$ s, using the total binding free energies, ΔG , as the sole descriptor variable. A good correlation was found between the inhibitory potencies and the predicted binding free energies (eq 2), and this relationship is also graphically shown in Figure 4.

$$\log IC_{50} = -2.968 - 0.763 \times \Delta G \quad (n = 27, r = 0.927, r^2 = 0.860, F_{1,25} = 162.240, s = 0.188) \quad (2)$$

It is obvious that there would be nearly 1.4 kcal/mol difference in binding free energy if there is one order numerical difference in the inhibitory potency (IC_{50}). As listed in Table 4, the decreasing amount in binding free energy caused by substitution from the meta to para position relative to the hydroxyl group at Ar_1 is greater than that of substitution from the meta to ortho position. The methyl substitution at the meta position of the Ar_2 group may increase the binding affinity as compared with that at the para position as judged from the amount of binding free energy, which is in agreement with the data of the inhibitory potency (Table 4).

The above relationship together with the interacting mode of AHPBAs with HIVPR can enhance and complement the comprehension for the binding-inhibitory potency relations deduced from experimental data.^{10,46-49} The structure-based thermodynamic analyses, using the isothermal titration calorimetry and other biological assays,^{10,47-48} had demonstrated the linkage between the binding energetics of inhibitors and the structural stability of HIVPR. The dissection of the thermodynamic forces⁴⁹ indicated that the high binding affinity of an

inhibitor with HIVPR came from the favorable binding free energy. The structural and energetic explanation herein is consistent with the viewpoints from these experimental results. The values of the predicted binding free energies for AHPBAs (Table 3 and Figure 4) are at the same level with the experimental data.⁴⁷⁻⁴⁹ Beyond the experimental studies, it is clearly illustrated for the positional contribution of the substitution groups to the binding of AHPBAs with HIVPR and the resulting inhibitory potency against HIVPR.

The sophisticated method for the calculation of binding free energy is the free energy perturbation (FEP) approach.^{50,51} However, the FEP approach is time-consuming; thus, it cannot be extended to predict the binding affinities for a large set of molecules. Dominy et al.¹¹ developed an empirical protocol for binding free energy prediction based on the generation of protein-ligand complex ensembles and applied this method in protein-ligand binding simulation of the HIV/FIV protease system. As compared with the FEP approach,^{50,51} this empirical method saves a lot of computational expense. It is still time-consuming if one uses this method in predicting the binding affinities of a series of molecules, for each ligand has to be docked into the conformational ensembles derived from an amount of X-ray crystal structures of the protein-ligand complex or from the molecular dynamics simulations. Automated molecular docking can identify the binding conformation and predict the binding affinity very quickly; therefore, it can be applied in constructing the prediction model for a series of molecules in a tolerable time, as indicated above that the inhibitory potency correlates well with the AutoDock predicted binding free energy (eq 2 and Figure 4). This relationship suggests that those potential HIVPR inhibitors exhibiting stronger binding free energies using this paradigm would therefore be expected to have greater efficacy toward inhibitory action.

3. 3D-QSAR Models. 3.1. CoMFA. Although CoMFA is not able to appropriately describe all of the binding force, being based principally on standard steric and electrostatic molecular fields to model substrate-enzyme interactions, it is still a widely used tool for the study of QSAR at the 3D level. The major objective of CoMFA analysis about AHPBAs is to find the best predictive model within the system. PLS analysis results based on a least-squares fit are listed in Table 4, which shows that all of the statistical indexes are reasonably high. Table 5 is compiled with the predicted activities of these 27 AHPBAs by the 3D-QSAR model vs their experimental inhibitory potencies ($-\log IC_{50}$ s). As listed in Table 4, for a CoMFA model with a r_{cv}^2 value of 0.613 for five components, a conventional r^2 of 0.978 is obtained based on the binding conformations and their alignment in the active site of HIVPR. The linear relationship shown in Figure 5 indicates that the fitting power is rational potent and the predictive ability is satisfactory.

3.2. CoMSIA. CoMSIA analysis results are also summarized in Table 4. A CoMSIA model with an r_{cross}^2 value of 0.530 for six components and a conventional r^2 of 0.970 is obtained. These data demonstrate that the CoMSIA model is also fairly predictive, and the predicted inhibitory potencies of AHPBA are listed in Table 5 and also shown in Figure 5. The highly conventional

Table 5. Predicted Activities (PA) vs Experimental Activities (EA, $-\log\text{IC}_{50}$) and Residues (δ) by CoMFA, CoMSIA, and HQSAR

compd	EA	CoMFA		CoMSIA		HQSAR	
		PA	δ	PA	δ	PA	δ
1	8.10	8.18	-0.08	8.20	-0.10	7.99	0.11
2	8.89	8.98	0.09	8.79	0.10	8.93	-0.04
3	8.77	8.84	-0.07	8.92	-0.15	8.88	-0.11
4	8.60	8.66	-0.06	8.64	-0.04	8.65	-0.05
5	8.46	8.34	0.12	8.31	0.15	8.41	0.05
6	8.72	8.79	-0.07	8.68	0.04	8.78	-0.06
7	8.68	8.70	-0.02	8.68	0.00	8.69	-0.01
8	8.34	8.37	-0.03	8.40	-0.06	8.45	-0.11
9	8.20	8.20	0.00	8.18	0.02	8.26	-0.06
10	8.41	8.36	0.05	8.39	0.02	8.40	0.01
11	8.60	8.62	-0.02	8.64	-0.04	8.44	0.16
12	8.89	8.98	-0.09	8.96	-0.07	8.81	0.08
13	7.50	7.45	0.05	7.42	0.08	7.50	0.00
14	8.10	8.12	-0.02	8.14	-0.04	8.24	-0.14
15	8.44	8.39	0.05	8.45	-0.01	8.34	0.10
16	7.30	7.38	-0.08	7.29	0.01	7.35	-0.05
17	7.46	7.38	0.08	7.42	0.04	7.44	0.02
18	8.92	8.94	-0.02	8.95	-0.03	8.98	-0.06
19	8.49	8.50	-0.01	8.52	-0.03	8.58	-0.09
20	9.10	9.07	0.03	9.04	0.06	8.96	0.14
21	8.55	8.54	0.01	8.56	-0.01	8.62	-0.07
22	8.92	8.81	0.11	8.80	0.12	8.90	0.02
23	9.10	9.01	0.09	8.99	0.11	8.95	0.15
24	7.59	7.71	-0.12	7.70	-0.11	7.70	-0.11
25	7.96	7.86	0.10	7.87	0.09	7.87	0.09
26	7.92	7.90	0.02	7.94	-0.02	7.85	0.07
27	8.44	8.43	0.01	8.42	0.02	8.54	-0.10
1*	6.00	6.18	-0.18	5.96	0.04	6.21	-0.21
2*	6.00	6.08	-0.08	5.93	0.07	5.91	0.09
3*	7.41	7.21	0.20	7.39	0.02	7.43	-0.02
4*	8.05	8.08	-0.03	8.15	-0.10	8.06	-0.01
5*	8.82	8.72	0.10	8.68	0.14	8.90	-0.08
6*	8.47	8.41	0.06	8.57	0.10	8.49	-0.02
7*	8.89	8.95	-0.06	8.94	-0.05	8.79	0.10
8*	8.27	8.28	-0.01	8.33	-0.06	8.27	0.00
9*	7.85	7.84	0.01	7.93	-0.08	7.89	-0.04
kni272*	8.20 ⁴⁶	8.07	0.13	8.17	0.03	8.14	0.06

* Compounds that were not included in the construction of the 3D-QSAR models.

r^2 results relating to five different descriptor variables (steric, electrostatic, hydrophobic, and hydrogen bond donor and acceptor) (Table 4) illustrate that these variables are necessary not only to fully describe the field properties around the AHPBA molecules but also to fully describe the interaction mode of AHPBAs with HIVPR.

3.3. HQSAR. Table 4 also shows a summary of the HQSAR calculation results. These data show that the least standard error occurs at a cross-validated r^2 (q^2) of 0.717 with five optimal components. The hologram that gives the lowest standard error has a length of 307. The PLS analysis yields a conventional r^2 of 0.950 for the studied compounds. The predicted inhibitory potencies of AHPBAs against HIVPR are also listed in Table 5, and their correlation is shown in Figure 5. It is important to have a QSAR technique that offers not only a consistent and reproducible prediction but also a fast and convenient procedure. The HQSAR model in the study appears well-suited for such application.

3.4. Testing of 3D-QSAR Models. To test the stability and predictive ability of the 3D-QSAR results of AHPBAs, nine analogous compounds¹⁴⁻¹⁷ together with compound kni272,²⁸ which was not included in the construction of CoMFA, CoMSIA, and HQSAR models, were selected as a set of testing for validation. The

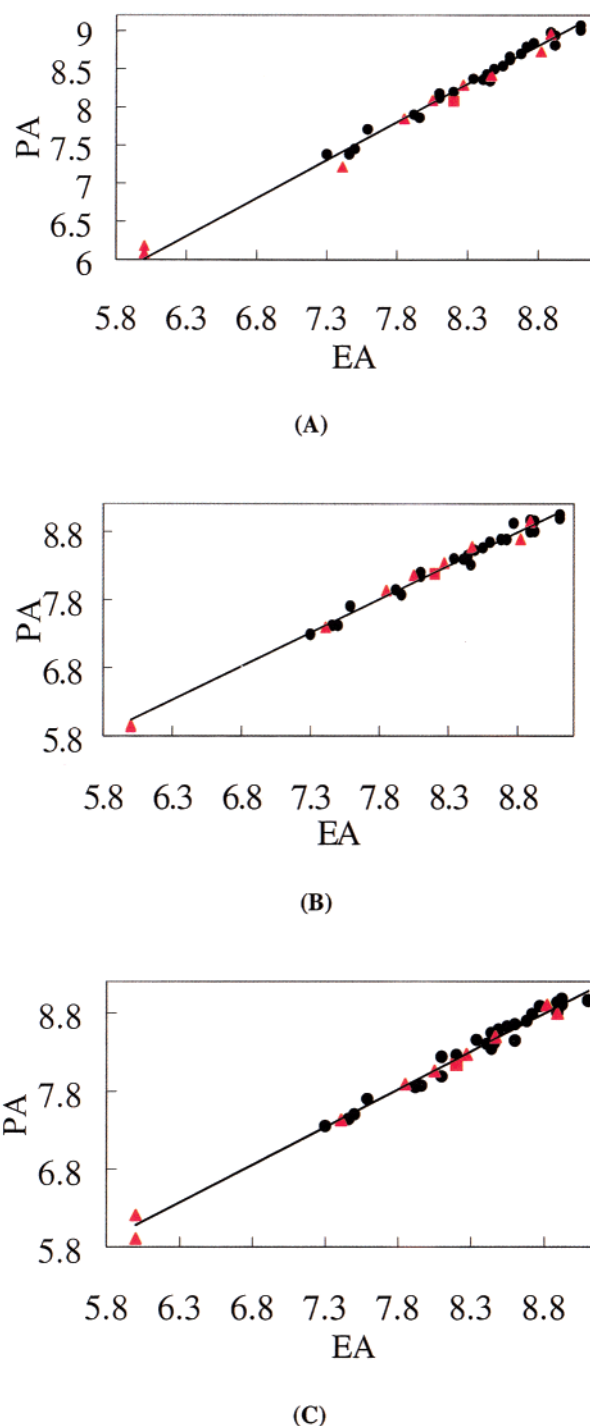


Figure 5. Correlation between the predicted activities (PA) by CoMFA (A), CoMSIA (B), and HQSAR (C) models and the experimental inhibitory potencies ($-\log\text{IC}_{50}$) (●, compounds of the training set; ▲, compounds of the testing set; ■, kni272).^{28,46}

results are simultaneously shown in Table 5 (star-labeled compound numbers) and Figure 5 (in triangle and square pattern-labeled symbols), and the predicted $-\log\text{IC}_{50}$ values are in good agreement with the experimental data in a statistically tolerable error range. To investigate structural differences of binding mode between the testing set of compounds and the training set, automated molecular docking was performed for the testing set using the same docking method as that of the training set. The geometrical parameters and the predicted

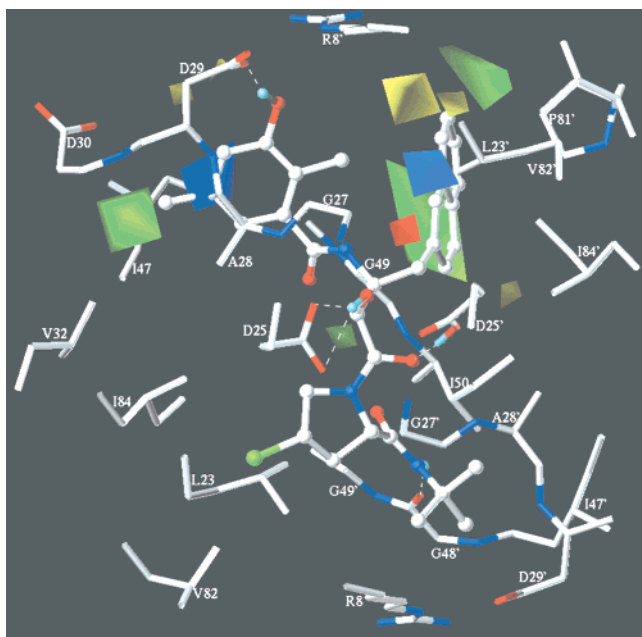


Figure 6. CoMFA contour maps as compared with the structural topology of the binding site in the AHPBA–HIVPR complex; only the residues within 5 Å around the inhibitor (compound **20**) are shown in the stick style.

binding free energies for these compounds were also compiled in Tables 2 and 3 and graphically shown in Figures 2C and 4, respectively. As listed in Table 2 and shown in Figure 2C, the three torsion angles and the conformational RMSD values as compared with kni272²⁸ are in the same levels as that of the training set. The torsion angle τ_3 for compounds **1***–**3***, which indicates the relative position of the aromatic ring in the Ar₁ group and the adjacent carbonyl amide backbone, is almost 30 degrees less than that of all others. This means that the energy consumed for the conformational change from the coplanar to out-of-planar state (binding conformation) of these three compounds is much less than that of the 3-OH's of the Ar₁ compound. In other words, the binding energies for compounds **1***–**3*** must be much lower. Inspecting the feature of the binding conformation of compounds **1***–**3***, one intramolecular hydrogen bond is formed between the –OH or the –NH₂ of the Ar₁ group and the oxygen atom of the adjacent amide carbonyl group. Meanwhile, the typical hydrogen bond between the –OH of the Ar₁ group of AHPBAs and the O^{δ1} of the Asp29 of HIVPR could not be formed. This may be the structural and energetic source for the great decrease of binding affinities and therefore the lower inhibitory potencies for compounds **1***–**3***. The much higher level of predicted binding free energies shown in Table 3 and Figure 4 is the direct reflection and testimony of the difference in the binding mode for compounds **1***–**3*** as compared with other inhibitors.

4. CoMFA Contour Map and Comparison with HIVPR Topology. The 3D “contour plots” produced by CoMFA are shown in Figure 6. Colored polyhedras in the map show these areas in 3D space where changes in the field values for AHPBAs correlate strongly with concomitant changes in inhibitory potencies. Detrimental and beneficial steric interactions are respectively displayed in yellow and green contours, while blue and red contours illustrate the regions of desirable positive

and negative electrostatic interactions. Some large regions of green contour around the outside edge of the Ar₂ group suggest that more bulky substituents in these positions will significantly improve the inhibitory potencies. The yellow polyhedra near the inside edge of the para position of the above aromatic ring indicates that more steric bulk is unfavorable for the inhibitory potencies. The blue contours near the Ar₁ and Ar₂ group suggest that positively charged substituents might increase the biological activity. The small red polyhedra around the Ar₂ group indicates that high electron density might play a favorable role in inhibitory potencies.

Combining the CoMFA contour map with the topology of the HIVPR 3D structural binding site for AHPBAs, several insights into the binding of AHPBAs with HIVPR, which is described in the “interacting mode” section, can also readily be observed from the CoMFA map. The field property not only coincides well with the environmental characteristics of the binding pocket but also indicates that some further structural modification of AHPBAs could be found. Most of the amino acids around the AHPBAs in the binding pocket are hydrophobic in nature (Figure 6); this is consistent with the CoMFA results about the relative field attribute. The colored polyhedras of CoMFA located in the cavity of the binding pocket are a direct index for the kinds and magnitudes of the substituents selection in the process of AHPBA analogues synthesis.

Furthermore, some SARs of AHPBAs could highlight the consistency between the 3D-QSAR results and the complementary features of AHPBAs with the binding site of HIVPR. Introducing a hydrophobic substituent to the meta position of the hydroxyl group at Ar₁ significantly increases the binding affinity of AHPBAs with HIVPR.¹⁷ The green polyhedra around the hydroxyl group of Ar₁ coincides with the hydrophobic pocket enveloping the Ar₁ group. The meta substituent could be enlarged to some extent in order to intensify the interaction between this part of Ar₁ and the side chains of residues Val32, Ile47, and Ile84 of HIVPR. This may be the reason why the inhibitory activities of compounds **2**, **3**, **6**, **7**, **12**, **18**, **20**, and **22** are higher than other compounds that do not contain such substituents. The meta substitution of a methyl group instead of fluorine at Ar₁ is more suitable because of the more hydrophobic than electrostatic interaction requirement of this subsite; thus, the inhibitory potencies of compounds have the order of **2** > **3** and **6** > **7**. The methyl group at the ortho position of –OH in Ar₁ (Table 1) interacts with the aromatic ring of Ar₂ in a mode of alkane– π interaction³⁷ (Figures 1, 3, and 6). This kind of intramolecular interaction takes a symmetrical 3D position with the alkane– π interaction between the aromatic ring of Ar₂ and the side chains of Val82' and Ile84' in HIVPR (Figure 3). These alkane– π interactions make the molecular energy of AHPBA lower, and it is beneficial to the AHPBA–HIVPR complex formation.

As one can see from Figure 6, the local hydrophobic pocket at the S₁ subsite is large enough to envelop a relatively large volume group. The more bulky aromatic substitution could interact better with the side chains of residues Leu23', Ile50, Pro81', Val82', and Ile84' of HIVPR and therefore increase the inhibitory potencies

of AHPBAs. The two large green polyhedras situated around the Ar₂ group could demonstrate this point of view, and the meta and/or para substitutions are the best choice to intensify this local hydrophobic interaction. Therefore, it is natural that the inhibitory activities of the compounds in Table 1 have the order **19** > **1**, **20** > **2**, **22** > **7**, **11** > **9**, **12** > **6**, and **14** > **16**.

Conclusion

We have obtained not only the probable binding conformations but also the reasonable prediction of binding free energies of AHPBAs with HIVPR employing the LGA algorithm of the AutoDock 3.0 program.³⁰ Modeling results indicate that the binding free energies of AHPBAs calculated by this method correlate very well with the reported inhibitory potencies against HIVPR^{14–17} and provide a structural and energetic explanation for the differences in the binding affinities of AHPBAs with HIVPR. On the basis of the binding conformations of AHPBAs, we have developed stable and predictive 3D-QSAR models with acceptable r_{cross}^2 values by undertaking CoMFA, CoMSIA, and HQSAR techniques, and these models could be mapped back to the structural topology of the active site in HIVPR. This leads to a better understanding of important AHPBA–HIVPR interactions and thus provides guidelines for the structural modifications of the inhibitors and a predictive model for scoring novel synthetic candidates.

Typically, structure-based design is focused on the elucidation of enzyme–substrate interactions but does not always lead to predictive models. On the other hand, 3D-QSAR models do not necessarily reflect topological features of the protein structure. These models are generally constructed using alignment rules, which are not always consistent with the characteristics of the binding conformations. In this study, we successfully combined these two approaches. The 3D-QSAR results allow focus on those regions, where electrostatic, steric, or hydrophobic effects have a dominant role in AHPBA–HIVPR interactions. The predictive ability testing for the models has validated their robustness, so the application of these models for quantitative prediction of inhibitory potencies against HIVPR is possible within a structurally limited range. Hence, for new candidates as potential HIVPR inhibitors, reliable inhibitory activities can be computed by “interpolation”, and less reliable IC₅₀'s by “extrapolation” might be obtained for candidates with lower structural similarity to the training set molecules.

Acknowledgment. The authors are grateful for the financial support from the National Natural Science Foundation of China (Grant 29725203) and the State Key Program of Basic Research of China (Grant 1998051115). We also acknowledge Prof. Arthur J. Olson of the Scripps Research Institute in La Jolla, CA for his provision of the AutoDock 3.0 program.

References

- (1) Pearl, L. H.; Taylor, W. R. A structural model for the retroviral proteases. *Nature* **1987**, *329*, 351–354.
- (2) Ratner, L.; Haseltine, W.; Patarca, R.; Livak, K. J.; Starcich, B.; Josephs, S. F.; Doran, E. R.; Rafalski, J. A.; Whitehorn, E. A.; Baumeister, K. Complete nucleotide sequence of the AIDS virus, HTLV-III. *Nature* **1985**, *313*, 277–84.

- (3) Seelmeier, S.; Schmidt, H.; Turk, V.; von der Helm, K. Human immunodeficiency virus has an aspartic-type protease that can be inhibited by pepstatin A. *Proc. Natl. Acad. Sci. U.S.A.* **1988**, *85* (18), 6612–6616.
- (4) Appett, K. Crystal structures of HIV-1 protease–inhibitors complexes. *Perspect. Drug Discovery Des.* **1993**, *1*, 23–48.
- (5) Kohl, N. E.; Emimi, E. A.; Schleich, W. A.; Davis, L. J.; Heimbach, J. C.; Dixon, R. A.; Scolnick, E. M.; Sigal, I. S. Active human immunodeficiency virus protease is required for viral infectivity. *Proc. Natl. Acad. Sci. U.S.A.* **1988**, *85*, 4686–4690.
- (6) McQuade, T. J.; Tomasselli, A. G.; Liu, L.; Karacostas, V.; Moss, B.; Sawyer, T. K.; Heinrikson, R. L.; Tarpley, W. G. A synthetic HIV-1 protease inhibitor with antiviral activity arrests HIV-like particle maturation. *Science* **1990**, *247*, 454–456.
- (7) Pyring, D.; Lindberg, J.; Rosenquist, A.; Zuccarello, G.; Kvarnstrom, I.; Zhang, H.; Vrang, L.; Unge, T.; Classon, B.; Hallberg, A.; Samuelsson, B. Design and synthesis of potent C(2)-symmetric diol-based HIV-1 protease inhibitors: effects of fluoro substitution. *J. Med. Chem.* **2001**, *44* (19), 3083–3091.
- (8) Rozzelle, J. E.; Dauber, D. S.; Todd, S.; Kelle, R.; Craik, C. S. Macromolecular inhibitors of HIV-1 protease. *J. Biol. Chem.* **2000**, *275*, 7080–7086.
- (9) Lee, T.; Laco, G. S.; Torbett, B. E.; Fox, H. S.; Lerner, D. L.; Elder, J. H.; Wong, C. H. Analysis of the s3 and s3' subsite specificities of feline immunodeficiency virus (FIV) protease: development of a broad-based protease inhibitors efficacious against FIV, SIV, and HIV in vitro and ex vivo. *Proc. Natl. Acad. Sci. U.S.A.* **1998**, *95*, 934–944.
- (10) Todd, J. M.; Freire, E. The effect of inhibitor binding on the structural stability and cooperativity of the HIV-1 protease. *Proteins: Struct., Funct., Genet.* **1999**, *36*, 147–156.
- (11) Dominy, B. N.; Brooks, C. L., III. Methodology for protein–ligand binding studies: application to a model for drug resistance, the HIV/FIV protease system. *Proteins: Struct., Funct., Genet.* **1999**, *36*, 318–331.
- (12) Hagen, S. E.; Domagala, J.; Gajda, C.; Lovdahl, M.; Tait, B. D.; Wise, E.; Holler, T.; Hupe, D.; Nouhan, C.; Urumov, A.; Zeikus, G.; Zeikus, E.; Lunney, E. A.; Pavlovsky, A.; Gracheck, S. J.; Saunders, J.; VanderRoest, S.; Brodfuehrer, J. 4-Hydroxy-5,6-dihydroxyprones as inhibitors of HIV protease: the effect of heterocyclic substituents at C-6 on antiviral potency and pharmacokinetic parameters. *J. Med. Chem.* **2001**, *44* (14), 2319–2332.
- (13) Hong, L.; Zhang, X. J.; Foundling, S.; Hartsuck, J. A.; Tang, J. Structure of a G48H mutant of HIV-1 protease explains how glycine-48 replacements produce mutants resistant to inhibitor drugs. *FEBS Lett.* **1997**, *420*, 11–16.
- (14) Sakurai, M.; Higashida, S.; Sugano, M.; Komai, T.; Yagi, R.; Ozawa, Y.; Handa, H.; Nishigaki, T.; Yabe, Y. Structure–activity relationships of HIV-1 PR inhibitors containing AHPBA. *Bioorg. Med. Chem.* **1994**, *2*, 807–825.
- (15) Komai, T.; Higashida, S.; Sakurai, M.; Nitta, T.; Kasuya, A.; Miyamaoto, S.; Yagi, R.; Ozawa, Y.; Handa, H.; Mohri, H.; Yasuoka, A.; Oka, S.; Nishigaki, T.; Kimura, S.; Shimada, K.; Yabe, Y. Structure–activity relationships of HIV-1 PR inhibitors containing AHPBA?II. Modification of pyrrolidine ring at P1' proline. *Bioorg. Med. Chem.* **1996**, *4*, 1365–1377.
- (16) Takashiro, E.; Watanabe, T.; Nitta, T.; Kasuya, A.; Miyamoto, S.; Ozawa, Y.; Yagi, R.; Nishigaki, T.; Shibayama, T.; Nakagawa, A.; Iwamoto, A.; Yabe, Y. Structure–activity relationship of HIV-1 protease inhibitors containing AHPBA. Part III: Modification of P2 site. *Bioorg. Med. Chem.* **1998**, *6*, 595–604.
- (17) Takashiro, E.; Hayakawa, I.; Nitta, T.; Kasuya, A.; Miyamoto, S.; Ozawa, Y.; Yagi, R.; Yamamoto, I.; Shibayama, T.; Nakagawa, A.; Yabe, Y. Structure–activity relationship of HIV-1 protease inhibitors containing α -hydroxy- β -amino acids. Detailed study of P1 site. *Bioorg. Med. Chem.* **1999**, *7*, 2063–2072.
- (18) Kaldor, S. W.; Kalish, V. J.; Davies, J. F.; Shetty, B. V.; Fritz, J. E.; Appelt, K.; Burgess, J. A.; Campanale, K. M.; Chirgadze, N. Y.; Clawson, D. K.; Dressman, B. A.; Hatch, S. D.; Khalil, D. A.; Kosa, M. B.; Lubbehusen, P. P.; Muesing, M. A.; Patick, A. K.; Reich, S. H.; Su, K. S.; Tatlock, J. H. Viracept (nelfinavir mesylate, AG1343): a potent, orally bioavailable inhibitor of HIV-1 protease. *J. Med. Chem.* **1997**, *40*, 3979–3985.
- (19) Ringhofer, S.; Kallen, J.; Dutzler, R.; Billoch, A.; Visser, A. J. W. G.; Scholz, D.; Steinhäuser, O.; Schreiber, H.; Auer, M.; Kungl, A. J. X-ray structure and conformational dynamics of the HIV-1 protease in complex with the inhibitor sdz283–910: agreement of time-resolved spectroscopy and molecular dynamics simulations. *J. Mol. Biol.* **1999**, *286*, 1147–1159.
- (20) Gupta, S. P.; Babu, M. S. Quantitative structure–activity relationship studies on cyclic cyanoguanidines acting as HIV-1 protease inhibitors. *Bioorg. Med. Chem.* **1999**, *7*, 2549–2553.
- (21) Jiang, H. L.; Chen, K. X.; Tang, Y.; Chen, J. Z.; Li, Q.; Wang, Q. M.; Ji, R. Y. Molecular modeling and 3D-QSAR studies on the interaction mechanism of tripeptidyl thrombin inhibitors with human a-thrombin. *J. Med. Chem.* **1997**, *40*, 3085–3090.

- (22) Cramer, M.; Cramer, R. D., III; Jones, D. M. Comparative molecular field analysis. 1. Effect of shape on binding of steroids to carrier proteins. *J. Am. Chem. Soc.* **1988**, *110*, 5959–5967.
- (23) Klebe, G.; Abraham, U.; Mietzner, T. Molecular similarity indices in a comparative analysis (CoMSIA) of drug molecules to correlate and predict their biological activity. *J. Med. Chem.* **1994**, *37*, 4130–4146.
- (24) Tong, W.; Lowis, D. R.; Perkins, R.; Chen, Y.; Welsh, W. J.; Goddette, D. W.; Heritage, T. W.; Sheehan, D. M. Evaluation of quantitative structure–activity relationship methods for large-scale prediction of chemicals binding to the estrogen receptor. *J. Chem. Inf. Comput. Sci.* **1998**, *38*, 669–677.
- (25) *Sybyl*, version 6.5; Tripos Associates: St. Louis, MO, 1998.
- (26) Frisch, M. J.; Trucks, G. W.; Schlegel, H. B.; Scuseria, G. E.; Robb, M. A.; Cheeseman, J. R.; Zakrzewski, V. G.; Montgomery, J. A., Jr.; Stratmann, R. E.; Burant, J. C.; Dapprich, S.; Millam, J. M.; Daniels, A. D.; Kudin, K. N.; Strain, M. C.; Farkas, O.; Tomasi, J.; Barone, V.; Cossi, M.; Cammi, R.; Mennucci, B.; Pomelli, C.; Adamo, C.; Clifford, S.; Ochterski, J.; Petersson, G. A.; Ayala, P. Y.; Cui, Q.; Morokuma, K.; Malick, D. K.; Rabuck, A. D.; Raghavachari, K.; Foresman, J. B.; Cioslowski, J.; Ortiz, J. V.; Stefanov, B. B.; Liu, G.; Liashenko, A.; Piskorz, P.; Komaromi, I.; Gomperts, R.; Martin, R. L.; Fox, D. J.; Keith, T.; Al-Laham, M. A.; Peng, C. Y.; Nanayakkara, A.; Gonzalez, C.; Challacombe, M.; Gill, P. M. W.; Johnson, B. G.; Chen, W.; Wong, M. W.; Andres, J. L.; Head-Gordon, M.; Replogle, E. S.; Pople, J. A. *Gaussian 98*; Gaussian, Inc.: Pittsburgh, PA, 1998.
- (27) Purcel, W. P.; Singer, J. A. *J. Chem. Eng. Data* **1967**, *12*, 235–246. Details of the implementation are given in *Sybyl 6.5 Theory Manual*; Tripos: St. Louis, MO, 1998; p 69.
- (28) Baldwin, E. T.; Bhat, T. N.; Gulnik, S.; Liu, B.; Topol, I. A.; Kiso, Y.; Mimoto, T.; Mitsuya, H.; Erickson, J. W. Structure of HIV-1 protease with KNI-272, a tight-binding transition-state analogue containing allophenylnorstatine. *Structure* **1995**, *3* (6), 581–590.
- (29) *InsightII*, version 98; Molecular Simulation Inc.: California, 1998.
- (30) Morris, G. M.; Goodsell, D. S.; Halliday, R. S.; Huey, R.; Hart, W. E.; Belew, R. K.; Olson, A. J. Automated docking using Lamarckian genetic algorithm and empirical binding free energy function. *J. Comput. Chem.* **1998**, *19*, 1639–1662.
- (31) Solis, F. J.; Wets, R. J. B. Minimization by random search techniques. *Maths Opera. Res.* **1981**, *6*, 19–30.
- (32) Weiner, S. J.; Kollman, P. A.; Case, D. A.; Singh, C.; Ghio, G.; Alagona, S.; Profeta, P.; Weiner, P. *J. Am. Chem. Soc.* **1984**, *106*, 765–784. Details of the implementation are given in *Sybyl 6.5 Theory Manual*; Tripos: St. Louis, MO, 1998; p 441.
- (33) Morris, G. M.; Goodsell, D. S.; Huey, R.; Olson, A. J. Distributed automated docking of flexible ligands to proteins: parallel applications of AutoDock 2.4. *J. Comput.-Aided Mol. Des.* **1996**, *10*, 293–304.
- (34) Ghose, A. K.; Viswanadhan, V. N.; Wendoloski, J. J. A knowledge-based approach in designing combinatorial or medicinal chemistry libraries for drug discovery. 1. A qualitative and quantitative characterization of known drug databases. *J. Comb. Chem.* **1999**, *1*, 55–68.
- (35) Thompson, W. J.; Fitzgerald, P. M.; Holloway, M. K.; Emini, E. A.; Darke, P. L.; McKeever, B. M.; Schleif, W. A.; Quintero, J. C.; Zugay, J. A.; Tucker, T. J.; Schwering, J. E.; Homnick, C. F.; Nunberg, J.; Springer, J. P.; Juff, J. R. Synthesis and antiviral activity of a series of HIV-1 protease inhibitors with functionality tethered to the P1 or P1' phenyl substituents: X-ray crystal structure assisted design. *J. Med. Chem.* **1992**, *35*, 1685–1701.
- (36) Thanki, N.; Rao, J. K.; Foundling, S. I.; Howe, W. J.; Moon, J. B.; Hui, J. O.; Tomasselli, A. G.; Heinrichson, R. L.; Thaisrivongs, S.; Wlodawer, A. Crystal structure of a complex of HIV-1 protease with a dihydroxyethylene-containing inhibitor: comparisons with molecular modeling. *Protein Sci.* **1992**, *1*, 1061–1072.
- (37) Kim, K. S.; Tarakeshwar, P.; Lee, J. Y. Molecular clusters of π -systems: theoretical studies of structures, spectra, and origin of interaction energies. *Chem. Rev.* **2000**, *100*, 4145–4185.
- (38) Head-Gordon, M.; Pople, J. A. A Method for two-electron Gaussian integral and integral derivative evaluation using recurrence relations. *J. Chem. Phys.* **1988**, *89*, 5777.
- (39) POV-ray-Team; *POV-ray*, version 3; 1999 (www.povray.org).
- (40) Wallace, A. C.; Laskowski, R. A.; Thornton, J. M. LIGPLOT: A program to generate schematic diagrams of protein–ligand interactions. *Protein Eng.* **1995**, *8*, 127–134.
- (41) Erickson, J.; Neidhart, D. J.; VanDrie, J.; Kempf, D. J.; Wang, X. C.; Norbeck, D. W.; Plattner, J. J.; Rittenhouse, J. W.; Turon, M.; Wideburg, N.; Kohlbrenner, W. E.; Simmer, R.; Helfrich, R.; Paul, D. A.; Knigge, M. Design, activity, and 2.8 Å crystal structure of a C_2 symmetric inhibitor complexed to HIV-1 protease. *Science* **1990**, 527–533.
- (42) Rosin, C. D.; Belew, R. K.; Walker, W. L.; Morris, G. M.; Olson, A. J.; Goodsell, D. S. Coevolution and subsite decomposition for the design of resistance-evading HIV-1 protease inhibitors. *J. Mol. Biol.* **1999**, *287*, 77–92.
- (43) Nicholson, L. K.; Yamazaki, T.; Torchia, D. A.; Grzesiek, S.; Bax, A.; Stahl, S. J.; Kaufman, J. D.; Wingfield, P. T.; Lam, P. Y.; Jadhav, P. K. Flexibility and function in HIV-1 protease. *Nat. Struct. Biol.* **1995**, *2*, 274–280.
- (44) Rosin, C. D.; Belew, R. K.; Morris, G. M.; Olson, A. J.; Goodsell, D. S. Coevolutionary analysis of resistance-evading peptidomimetic inhibitors of HIV-1 protease. *Proc. Natl. Acad. Sci. U.S.A.* **1999**, *96*, 1369–1374.
- (45) Stahle, L.; Wold, S. Multivariate data analysis and experimental design in biomedical research. *Prog. Med. Chem.* **1988**, *25*, 291–338.
- (46) Mimoto, T.; Imai, J.; Kisanuki, S.; Enomoto, H.; Hattori, N.; Akaji, K.; Kiso, Y. Kynostatin (kni)-227 and –272, highly potent anti-HIV agents: conformationally constrained inhibitors of HIV protease containing allophenylnorstatine. *Chem. Pharm. Bull.* **1992**, *40* (8), 2251–2253.
- (47) Rick, S. W.; Topol, I. A.; Erickson, J. W.; Burt, S. K. Molecular mechanisms of resistance: free energy calculations of mutation effects on inhibitor binding to HIV-1 protease. *Protein Sci.* **1998**, *7* (8), 1750–1756.
- (48) Trylska, J.; Antosiewicz, J.; Geller, M.; Hodge, C. N.; Klabe, R. M.; Head, M. S.; Gilson, M. K. Thermodynamic linkage between the binding of protons and inhibitors to HIV-1 protease. *Protein Sci.* **1999**, *8* (1), 180–195.
- (49) Velazquez-Campoy, A.; Luque, I.; Todd, M. J.; Milutinovich, M.; Kiso, Y.; Freire, E. Thermodynamic dissection of the binding energetics of KNI-272, a potent HIV-1 protease inhibitor. *Protein Sci.* **2000**, *9* (9), 1801–1809.
- (50) Kollman, P. Free energy calculations: applications to chemical and biochemical phenomena. *Chem. Rev.* **1993**, *93*, 3 (7), 2395–2417.
- (51) Wang, L.; Duan, Y.; Stouten, P.; De Lucca, G. V.; Klabe, R. M.; Kollman, P. Does a diol cyclic urea inhibitor of HIV-1 protease bind tighter than its corresponding alcohol form? A study by free energy perturbation and continuum electrostatics calculations. *J. Comput.-Aided Mol. Des.* **2001**, *15* (2), 145–156.